Stochastic resonance with a mesoscopic reaction-diffusion system

Hitoshi Mahara,[1,2,*] Tomohiko Yamaguchi,[2] and P. Parmananda[1]
[1]*Department of Physics, India Institute of Technology Bombay, Powai, Mumbai 400076, India*
[2]*AIST, Higashi 1-1-1, Central 5-2, Tsukuba, Ibaraki, Japan*
(Received 12 November 2013; published 12 June 2014)

In a mesoscopic reaction-diffusion system with an Oregonator reaction model, we show that intrinsic noise can drive a resonant stable pattern in the presence of the initial subthreshold perturbations. Both spatially periodic and aperiodic stochastic resonances are demonstrated by employing the Gillespies stochastic simulation algorithm. The mechanisms for these phenomena are discussed.

DOI: 10.1103/PhysRevE.89.062913 PACS number(s): 05.45.−a, 82.20.Fd, 05.10.Gg, 05.40.−a

I. INTRODUCTION

Noise is regarded commonly as an undesirable disturbance that decreases the order of information. However, biological systems use noise efficiently and detect the otherwise undetectable signals [1–5]. This phenomenon, called stochastic resonance (SR), has been observed in and documented for numerous physical and chemical systems [6–17]. Zero-dimensional systems respond to a time series of subthreshold signals with noise [6–14]. Inhomogeneous two-dimensional systems detect spatial subthreshold information with noise [15–17]. The SR in inhomogeneous systems is deemed useful for image processing: a photo image is enhanced with noise in a nonlinear system [15], edge detection and phase separations have been demonstrated in a reaction-diffusion system [16,17].

Biological and chemical systems are influenced by either external or internal noises or by both. External noise comes from the environment and internal noise is induced by the fluctuations of the number of molecules. Chemical reactions can be described with the concentrations of chemical species and their corresponding differential equations with time if the number of molecules is large enough. However, these fluctuations due to noise become relatively large and unavoidable if the system and the number of molecules become small. These fluctuations in such scenarios are called intrinsic noise. Gillespie developed an algorithm to calculate the stochastic behavior of chemical reactions [18–20]. This algorithm was based on the chemical master equation and Monte Carlo methods and called the stochastic simulation algorithm (SSA). The SSA is used to investigate the influence of intrinsic noise in many systems [21–24]. While most of the reported studies involving SR have been carried out using external noise, some recent studies have employed intrinsic noise as well to show that the system described with the SSA can detect both periodic and aperiodic time series [21–24]. These results seem to indicate that intrinsic noise, if employed judiciously, is capable of exhibiting the SR phenomena.

The effect of intrinsic noise has also been studied in inhomogeneous systems that are called mesoscopic systems [25–32]. Several kinds of methods are developed to calculate these mesoscopic systems [27–32]. The SSA can also be modified and extended to investigate, numerically, the coupling between the chemical reactions and the intercellular kinetics in biological systems [25,26]. This extended method is called the reaction-diffusion SSA [33]. In this way, the influence of intrinsic noise was judiciously studied in mesoscopic reaction-diffusion systems. Because of this intrinsic noise, these systems show dynamical behaviors different from those observed in the corresponding macroscopic systems. For example, spatial pulses are pinned stably in a mesoscopic system, even though pulses move and an adjustment of the distances between the pulses occurs in the macroscopic counterpart [31]. In another case, inhomogeneous patterns appear in the parameter regions wherein only homogenous states can be observed for the corresponding macroscopic system [32]. However, to the best of our knowledge, there are no studies involving the SR with inhomogeneous system using the reaction-diffusion SSA. To reiterate, the SR with time, using the SSA, has already been reported [21–24]. In this paper, we demonstrate that a mesoscopic reaction-diffusion system shows stable response patterns that respond regularly to spatially periodic and aperiodic initial perturbations. We call these phenomena the spatially periodic stochastic resonance (S-PSR) and the spatially aperiodic stochastic resonance (S-ASR), following the previous paper of Ref. [24]. Furthermore, we discuss the mechanisms of the S-PSR and S-ASR.

II. MODEL SYSTEM

In the present work, we use the Oregonator model that shows the core chemical reactions of the Belousov-Zhabotinsky (BZ) reaction [34,35]. This model consists of the five reaction steps shown below:

$$A + Y \xrightarrow{k_1} X + P, \tag{1a}$$

$$X + Y \xrightarrow{k_2} 2P, \tag{1b}$$

$$A + X \xrightarrow{k_3} 2X + 2Z, \tag{1c}$$

$$2X \xrightarrow{k_4} A + P, \tag{1d}$$

$$B + Z \xrightarrow{k_5} fY, \tag{1e}$$

where k_1–k_5 are the reaction rate constants for the five chemical steps, respectively. f is a stoichiometric factor. The capital letters represent the numbers of molecules of chemical species:

*hitoshimahara@gmail.com

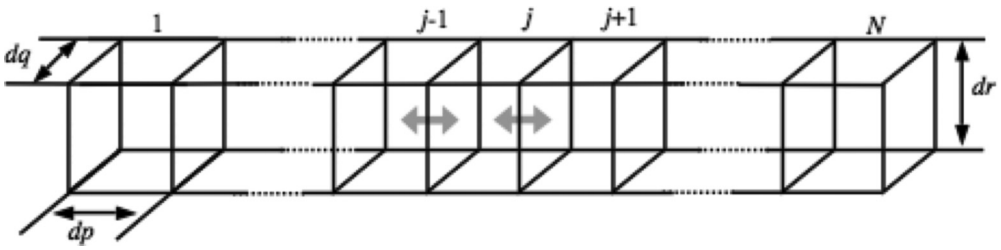

FIG. 1. The schematic view of the system with spatial coordinates p, q, and r. N cubic cells are the line in one dimension. The volume of each cell is $\Omega = dp \times dq \times dr$, $dp = dq = dr$. The molecules can go to the neighbor cells with diffusion.

$A = [BrO_3^-]$, $B = [CH_2(COOH)_2]$, $X = [HBrO_2]$, $Y = [Br^-]$, $Z = [Ce(IV)]$, and $P = [BrCH(COOH)_2]$. For simplicity, the numbers of molecules A, B, and P are kept constant. The other three for the chemical species X, Y, and Z are the variables.

A mesoscopic reaction diffusion system consists of cubic subsystems (cells) whose volume is $\Omega = dp \times dq \times dr$,$dp = dq = dr$. The N cubic cells are in line and the length of the system is $N \times dp$ (Fig. 1). Within the SSA, the propensity functions for the above five reactions in the jth cell are

$$\tilde{a}_{1,j} = k_1 A Y_j / \Omega, \tag{2}$$

$$\tilde{a}_{2,j} = k_2 X_j Y_j / \Omega, \tag{3}$$

$$\tilde{a}_{3,j} = k_3 A X_j / \Omega, \tag{4}$$

$$\tilde{a}_{4,j} = k_4 X_j (X_j - 1) / \Omega, \tag{5}$$

$$\tilde{a}_{5,j} = k_5 B Z_j / \Omega, \tag{6}$$

respectively. The suffix j indicates the cell number. In the present system, the molecules go to the next neighbor cells because of diffusion. Therefore, the following propensity functions for the diffusion of chemical species are calculated.

In the case that the molecules X, Y, and Z go to the left-side cell, respectively,

$$\tilde{a}_{6,j} = D_X X_j / (dp)^2, \tag{7}$$

$$\tilde{a}_{7,j} = D_Y Y_j / (dp)^2, \tag{8}$$

$$\tilde{a}_{8,j} = D_Z Z_j / (dp)^2. \tag{9}$$

In the case that the molecules X, Y, and Z go to the right-side cell, respectively,

$$\tilde{a}_{9,j} = D_X X_j / (dp)^2, \tag{10}$$

$$\tilde{a}_{10,j} = D_Y Y_j / (dp)^2, \tag{11}$$

$$\tilde{a}_{11,j} = D_Z Z_j / (dp)^2. \tag{12}$$

These propensity functions for diffusion have been calculated following the recipe provided in the work of Bernstein [30]. The D_X, D_Y, and D_Z are the diffusion coefficients of the chemical species X, Y, and Z, respectively. The system has no flux boundary conditions. Therefore, the molecules cannot go out through the right and left sides of the edge wall of the system.

We now discuss the implementation of the reaction-diffusion SSA in our model system. The states in every cell are known at the time t. First, the summation of the above propensity functions for each cell is calculated

$$S_j = \sum_i^{11} \tilde{a}_{i,j}. \tag{13}$$

The tie step, i.e., the waiting time δt for homogeneous system is calculated with this function. If this function is used for calculating the waiting time in the present system, this waiting time might differ from one cell to another. However, the waiting time in all of the cells should be the same for simulating the present system. Therefore, we introduce the 12th propensity function which corresponds to a no-event (neither reaction nor diffusion takes place) in the jth cell. We represent the largest one of the summation Eq. (13) as $S_{\max}$ and define the 12th propensity function for jth cell as follows:

$$\tilde{a}_{12,j} = S_{\max} - S_j. \tag{14}$$

The ith event (reaction, diffusion, or no-event) is chosen with a probability $\tilde{a}_{i,j}/S_{\max}$ in each cell, after a waiting time δt. This waiting time can be applied to every cell because of the existence of the 12th propensity function, Eq. (14). The waiting time is determined with the probability distribution function $P[\delta t \mid s(t)] = S_{\max} \exp(-S_{\max} \delta t)$. The state vector $s(t) = (X_1, Y_1, Z_1, X_j, Y_j, Z_j, \ldots, X_N, Y_N, Z_N)$ which has $3N$ components is updated to

$$s(t + \delta t) = s(t) + \sum_j^N v_j. \tag{15}$$

The vector $v_j = (dX_1, dY_1, dZ, \ldots, dX_j, dY_j, dZ_j, \ldots, dX_N, dY_N, dZ_N)$ depends on which event occurs in the jth cell. If the first reaction occurs in the jth cell, $dX_j = 1$ and $dY_j = -1$. The components becomes as follows in other cases: $dX_j = -1$ and $dY_j = -1$ for the second reaction, $dX_j = 1$ and $dZ_j = 2$ for the third reaction, $dX_j = -2$ for the fourth reaction, respectively. For the fifth reaction, dZ_j is -1 and dY_j is 2 with 70% probability or dY_j is 1 with 30% probability because the stoichiometric factor is not an integer and we use the parameter $f = 1.7$. If the diffusion events are selected in the jth cell, the component of v_j should be $dX_{j-1} = 1$ and $dX_j = -1$ for the sixth event, $dY_{j-1} = 1$ and

$dY_j = -1$ for the seventh event, $dZ_{j-1} = 1$ and $dZ_j = -1$ for the eighth event, $dX_{j+1} = 1$ and $dX_j = -1$ for the ninth event, $dY_{j+1} = 1$ and $dY_j = -1$ for the tenth event, and $dZ_{j+1} = 1$ and $dZ_j = -1$ for the 11th event. The components of the vector v_j that are not mentioned above are all zero for all the events. If the 12th event is selected in the jth cell all components of the vector v_j are equal to zero.

III. RESULTS

Here, we present numerical results that indicate that the mesoscopic reaction-diffusion system shows the S-PSR and S-ASR phenomena with SSA. The parameters are set to $k_1 = 0.274$, $k_2 = 1.11 \times 10^6$, $k_3 = 15.54$, $k_4 = 3.0 \times 10^3$, and $k_5 = 5.0$. To get stable patterns asymptotically, the diffusion coefficients are set to $D_X = 0.01$, $D_Y = 0.0$, and $D_Z = 100.0$. Here, we defined the unit of volume (u.v.) as the size that contains 1.0×10^8 molecules while the concentration is 1.0 mol/L. Therefore, we use the unit length (u.l.) that is $[1.0 \times 10^8/(N_A \times 1.0\text{mol/L})]^{1/3} = 0.166\,\mu\text{m}$, where $N_A = 6.022 \times 10^{23}\text{mol}^{-1}$ is the Avogadro number. The number of the chemical species A and B depends on the volume of the cubic cell. To keep the discussion simple, the concentrations for A and B are fixed to 0.4 and 0.1 M, respectively. Consequently, the number of molecules A and B are set to the nearest integer of $[(N_A[\text{mol}^{-1}] \times 0.4[\text{mol/L}])^{1/3}] \times \Omega[\text{u.v.}] = 0.4 \times \Omega \times 1.0x10^8[.]$ and $0.1 \times \Omega \times 1.0 \times 10^8[.]$, respectively. Hereafter, the concentrations of the chemical species x, y, and z are described with the unit that is the number per u.v. Furthermore, the unit of the diffusion coefficients was chosen to be $(\text{u.l.})^2\text{s}^{-1}$. The length of the system is about 920 u.l. (Fig. 1).

The present Oregonator system is an excitable media under the above conditions (see the Appendix). Subsequently, we modified the initial configuration of x spatially and the response of the system, represented with the spatial profile of the chemical concentration z, is recorded. The system shows a stable pulse in the z variable if a sufficiently large perturbation is provided in x. However, if the given perturbation does not exceed its threshold value the system goes back to the steady homogeneous state. The present system is given subthreshold perturbations and sometime responds to it with the help of intrinsic noise. We tune the amplitude of this intrinsic noise by varying Ω. The amplitude becomes larger as the volume decreases.

To quantitatively measure the agreement with the input and output spatial profiles, a power norm C_0, defined below, is computed as follows:

$$C_0 = \langle (x(p) - \langle x \rangle)(z(p) - \langle z \rangle) \rangle. \tag{16}$$

This is the modified version of the correlation function normally used for quantify time-dependent stochastic resonance phenomena [10,13,24]. Here, $\langle . \rangle$ denotes the spatial average. The profile $z(p)$ represents the final concentration of z at p. The profile $x(p)$ is the initial concentration at p when $t = 0$. Finally, this power norm is averaged over 50 trials for each volume. This means that, in reality, the norm is averaged over around 300 stimuli since five to seven stimuli exist in each trial.

A. Spatially periodic stochastic resonance

The S-PSR phenomena are observed in the mesoscopic reaction-diffusion system with the reaction-diffusion SSA. The initial conditions are chosen such that the numbers for the chemical species X, Y, and Z are the nearest integer of the fixed point $(x_{fp}, y_{fp}, z_{fp}) = (18.087, 1231.951, 449.712)$. Six square pulse perturbations are applied to X initially. The width of this pulse is 12 u.l. and the number X is perturbed to the lower nearest integer of $(19.0x_{fp}) \times \Omega$. All distances between these pulses are the same 138 u.l. These perturbations have almost the same profile as shown in Fig. 6(d) and can be considered as subthreshold for the present mesoscopic system since the corresponding macroscopic system shows no stable pulses for these conditions (see the Appendix).

The system is calculated 50 times for each values of Ω, i.e., different amplitudes of the intrinsic noise. Figure 2 shows the profiles of the initial perturbations and responses for three values: large, intermediate, and small. The system responds to only a few of the subthreshold perturbations in the case where the cell volumes are large, i.e., the noise intensity is low

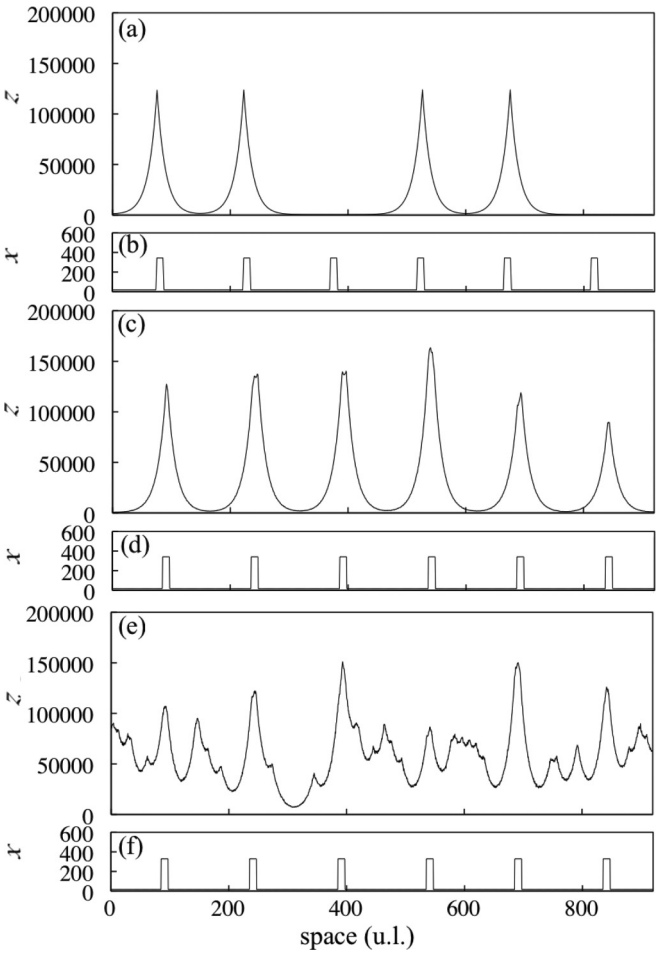

FIG. 2. Data for S-PSR. Panels (a), (c), and (e) show the final stable profile of z in the cases that spatially periodic perturbation are given initially as shown in panels (b), (d), and (f), respectively. The length and the volume of the cells are (a, b) $dp = 1.71$ u.l. and $\Omega = 5.04$ u.v.; (c, d) $dp = 0.63$ u.l. and $\Omega = 0.25$ u.v.; and (e, f) $dp = 0.4$ u.l. and $\Omega = 0.064$ u.v.

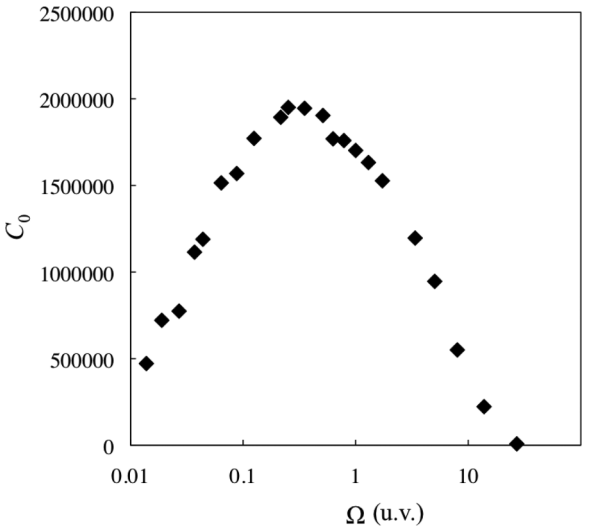

FIG. 3. The power norm C_0 against the cell volume Ω for S-PSR.

[Figs. 2(a) and 2(b)]. The system responds to almost all of the perturbations in the case that the cell volume is appropriate [Figs. 2(c) and 2(d)]. Many peaks appeared even in the region where the system is not perturbed, in the case where the cell volume is small [Figs. 2(e) and 2(f)]. Therefore, the output in the intermediate case for the optimal noise value becomes more correlated with the spatially periodic input perturbations as compared to other cases. From these initial and final profiles, we calculate C_0 using Eq .(16). The simulation results are extremely robust since for different initial conditions as well as different noise seeds similar features were observed. Figure 3 shows C_0 against Ω. This curve is almost unimodal and the maximal regularity corresponds to the optimum value of $\Omega = 0.25$. Thus the mesoscopic BZ reaction-diffusion system shows an S-PSR phenomenon.

B. Spatially aperiodic stochastic resonance

To demonstrate S-ASR, we use the same conditions as of the previous simulations except for the distance between the subthreshold perturbations. These distances are now chosen randomly between 48 to 228 u.l.. The width and the height of these perturbations are identical to the ones used before and therefore should be considered as subthreshold. The system is calculated 50 times for each volume Ω. Figure 4 shows the output profiles in the three cases: Ω is large, intermediate, and small. Analogous to the S-PSR, the system does not respond to several perturbations for the large volume case. The system responds to almost all the perturbations in the intermediate volume case. Many false or spuriouspeaks appear in the system for the case when the volume is small. Therefore, the output in the intermediate case becomes more correlated with the spatially aperiodic input perturbations as compared to other scenarios. From these initial and final profiles, we calculate C_0 using Eq. (16). Figure 5 shows the C_0 versus Ω graph. The maximal regularity corresponds to the optimum $\Omega = 0.42$, similar to that observed in S-PSR. Thus the mesoscopic BZ reaction-diffusion system shows an S-ASR phenomenon.

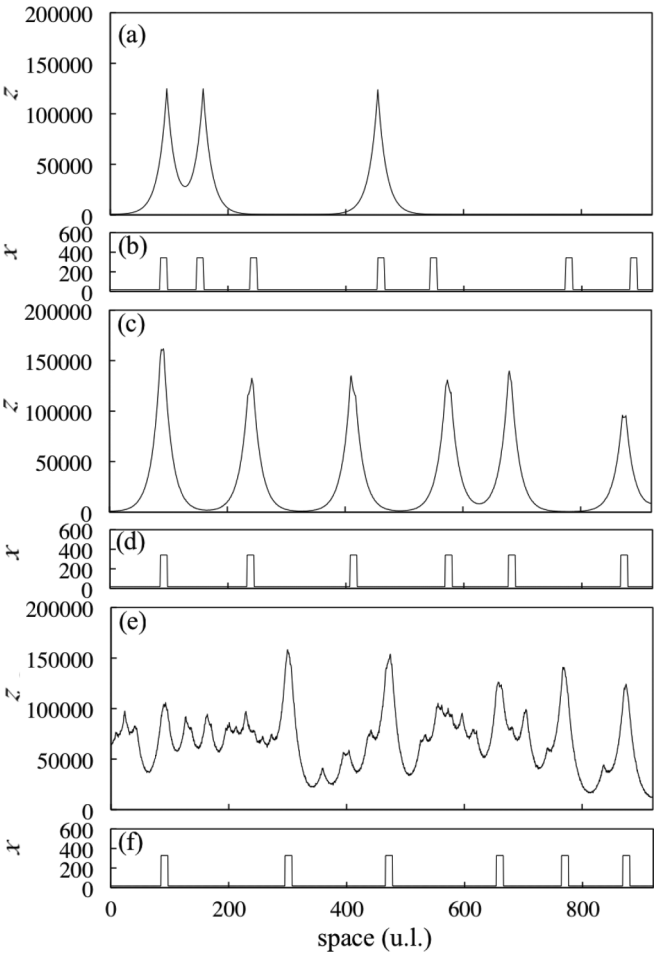

FIG. 4. Data for S-ASR. Panels (a), (c), and (d) show the final stable profile of z in the cases that spatially aperiodic perturbation are given initially as shown in panels (b), (d), and (f), respectively. The length and the volume of the cell are (a, b) $dp = 1.71$ u.l. and $\Omega = 5.04$ u.v.; (c, d) $dp = 0.75$ u.l. and $\Omega = 0.42$ u.v.; and (e, f) $dp = 0.4$ u.l. and $\Omega = 0.064$ u.v.

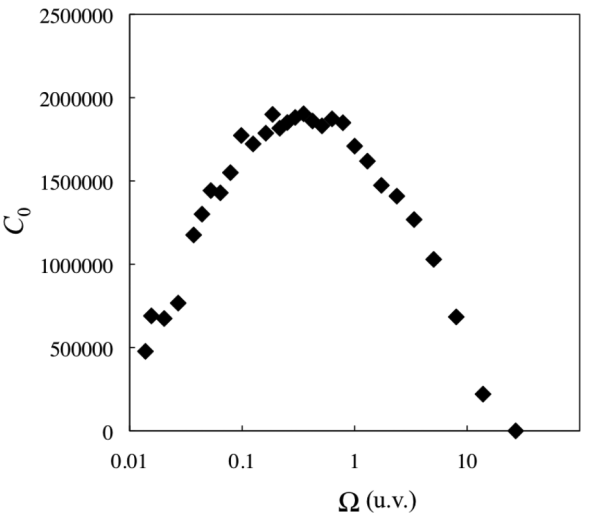

FIG. 5. The power norm C_0 against the cell volume Ω for S-ASR.

IV. SIMULATION DETAILS

The S-PSR and S-ASR phenomena are shown to exist in our mesoscopic system. The mechanism is similar to the other SR phenomena, reported in the literature. The noise regulates the probability of the system response to the subthreshold perturbations. This probability is low if the intrinsic noise amplitude is small, i.e., the cell volume is large. Therefore, the system responds to a few of the subthreshold perturbations. This probability increases as the noise amplitude increases and, therefore, the system shows a more correlated response to the subthreshold spatial pulse train. However, this probability increases also in the region that the system is not perturbed. Upon further augmentation of the noise amplitude, firings occur even in the region where the system is not perturbed. These firing phenomena induce extra pulses and the correlation between input and the output decreases. Consequently, unimodal curves of C_0 versus noise strength emerge and there exists an optimal noise amplitude where maximal correlation with the subthreshold perturbations is observed.

The model dynamics have a useful feature facilitating the emergence of the spatial stochastic resonance behavior. The present system has a solitary pulse solution which is different from the Turing patterns. The Turing pattern is a spatially periodic pattern that can be invoked with tiny levels of noise [36]. This implies that the mesoscopic reaction diffusion system would always show Turing patterns in the presence of intrinsic noise. Therefore, the system that shows Turing instability is not appropriate for studying the S-PSR and S-APSR phenomena. Moreover, Turing patterns have their own wavelengths and therefore the system might ignore periodic or aperiodic input spatial signals if their signal period is not coincident with its own wavelengths. Consequently, to observe SR with Turing instability, one needs to suppress all the features of Turing patterns. Unfortunately, we could not achieve this required suppression. As a result, we chose a system that shows a one pulse solution. Such solutions can be found in various models: the Gray-Scott model [37,38], Fitz-Hugh and Nagumo model [39], Gierer-Meinhardt model [40], and so on.

A solitary pulse has a repulsive feature with respect to other pulses in the continuous reaction diffusion system [38,40]. This feature induces autotuning of the distances between the pulses and, subsequently, a rearrangement of pulses occurs. Therefore, this feature is for the present SR phenomena. The motion of this pulse is suppressed if the diffusion coefficients are sufficiently small, i.e., the system is a discrete system [16,39]. Then the present system should be a discrete system, i.e., the system is not an approximation of the continuous system as mentioned in Ref. [33]. This means the present cubic cells should be real compartments. It is well known that the discrete system shows curious phenomena that cannot be observed in continuous systems with the same parameters [16,39,41–45]. These phenomena can be observed in an inhomogeneous system that consists of biological cells [44,45]. Furthermore, the discreteness of the molecule numbers can also induce this suppression of pulse movement [31]. In this paper, in conjunction with the fact that the molecular numbers are discrete, we chose the values of diffusion coefficients, especially D_X, smaller than the ordinal value whose order is $1.0 \sim 0.1 \times 10^{-5}\,\mathrm{cm^2 s^{-1}} = 3629 \sim 362.9\,(\mathrm{u.l.})^2\mathrm{s}^{-1}$. This ensures suppression of the pulse motion in our mesoscopic system and consequently the pulses stay eternally at the location where they begin to fire initially.

These special features ensure that the model system has the potential to induce stable resonant responses to spatially periodic or aperiodic input perturbations and therefore can exhibit the S-PSR and S-ASR phenomena.

V. CONCLUSION AND DISCUSSION

In the present work, we introduce the propensity function of no-event to calculate every cell with the same time increments in reaction-diffusion SSA. Subsequently, we succeeded in demonstrating the stochastic resonance against spatially periodic and aperiodic initial perturbations in a mesoscopic reaction-diffusion system. The system has an intrinsic noise whose strength is a function of the cell size. This noise enables the system to respond to subthreshold perturbations. The results of the correlation calculation indicate that an optimum volume exists where a maximal correlation between the input subthreshold spatial perturbations and the system response is observed. In simulation details, the mechanisms and some necessary conditions for the emergence of these phenomena are outlined. It is realized that the existence of one pulse solutions are important to invoke S-PSR and S-ASR. Our numerical results can be verified in any experimental system as long as it can exhibit a stable solitary pulse solution. For this to happen three conditions need to be met: (1) the system is excitable; (2) the ratio of the diffusion coefficients for the inhibitor and the activator satisfy the Turing instability condition; and (3) the

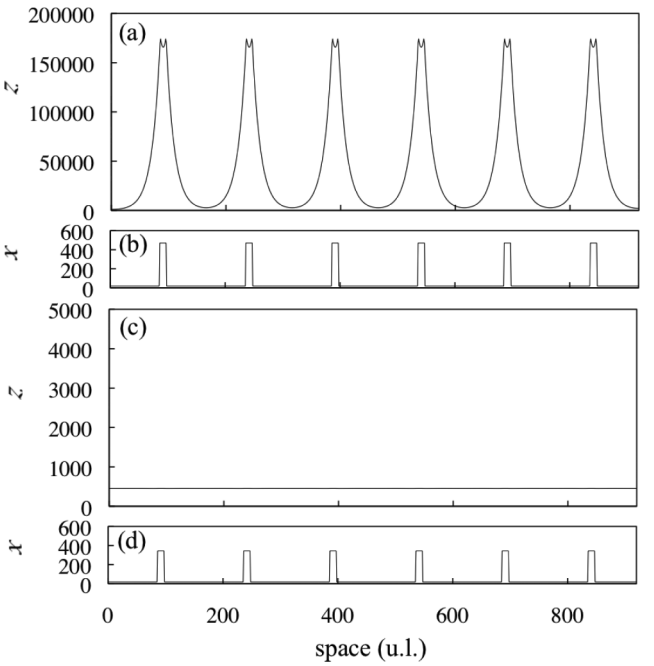

FIG. 6. Results in the macroscopic reaction diffusion system. (a) Final stable profile of z for initial profile of x in (b). The initial perturbations are overthreshold. The system responds to the initial perturabations and it shows the pulses' pattern. (c) Final stable profile of z for initial profile of x in (d). All of the perturbations are of subthreshold value and the system goes to a homogeneous state.

system is a desecrate system, i.e., the cubic cells should be real compartments like biological cells. It is well known that the BZ aerosol sodium bis(2-ethyl-1- hexyl) sulfosuccinate (AOT) system can show both steady patterns and the solitary pulse solution [46]. Therefore, the BZ-AOT experimental system is a suitable candidate system to test our predictions as it seems phenomenologically similar to the system chosen in our simulations if the discreteness of diffusion coupling can be realized. This experimental system with mesoscopic dimensions should be able to validate our numerical predictions.

ACKNOWLEDGMENTS

H.M. thanks T. Yamamoto for useful discussion. This work was supported by the Japanese Ministry of Education, Culture, Sports, Science, and Technology (MEXT) via a Grant-in-Aid for Scientific Research on Innovative Areas Emergence in Chemistry (Grant No. 20111007) and DST, India.

APPENDIX: MACROSCOPIC SYSTEM

The ordinal macroscopic reaction-diffusion system is described as

$$\frac{\partial x}{\partial t} = k_1 a y - k_2 x y + k_3 a x - 2k_4 x^2 + D_x \nabla^2 x, \quad \text{(A1)}$$

$$\frac{\partial y}{\partial t} = -k_1 a y + k_2 x y + k_5 f b z + D_y \nabla^2 y, \quad \text{(A2)}$$

$$\frac{\partial z}{\partial t} = 2k_3 a x - k_5 b z + D_z \nabla^2 z. \quad \text{(A3)}$$

Here a,b, and the variables represent the concentrations of each chemical species. The unit of the concentration is changed from mol/L to number per u.v. to compare easily to the results of the simulation in the main text. The system is calculated numerically with the fourth-order Runge-Kutta method and the finite difference discretization method is applied to the diffusion terms ($dp = 1.0, dt = 0.00001$).

The parameters are set identical to the ones used in the main text and the reaction-diffusion system is an excitable media. This system shows a stable pulse for superthreshold perturbations as shown in Fig. 6. Initially the system is set to the stable steady state $(x_{fp}, y_{fp}, z_{fp}) = (18.087, 1231.951, 449.712)$ uniformly. The concentration x is perturbed to $26.0 x_{fp}$ in six parts of the system in Fig. 2(b). The width of one perturbed region is 12 u.l. and the distance between these regions is 138 u.l. The stable pulses appear where the locations are subjected to superthreshold perturbations. On the other hand, the system becomes homogeneous if the perturbations are subthreshold [Figs. 6(c) and 6(d)]. The threshold value exists between $x = 20.0 \sim 21.0 x_{fp}$ for our numerical calculations.

[1] D. F. Russell, L. A. Wilkens, and F. Moss, Nature (London) **402**, 291 (1999).
[2] K. J. Douglass, L. Wilkens, E. Pantazelou, and F. Moss, Nature (London) **365**, 337 (1993).
[3] J. E. Levin and J. P. Miller, Nature (London) **380**, 165 (1996).
[4] J. J. Collins, T. T. Imhoff, and P. Grigg, J. Neurophysiol. **76**, 642 (1996).
[5] T. Mori and S. Kai, Phys. Rev. Lett. **88**, 218101 (2002).
[6] R. Benzi, A. Sutera, and A. Vulpiani, J. Phys. A **14**, L453 (1981).
[7] C. Nicolis, Tellus **34**, 1 (1982).
[8] J. J. Collins, C. C. Chow, and T. T. Imhoff, Phys. Rev. E **52**, R3321 (1995).
[9] J. J. Collins, C. C. Chow, A. C. Capela, and T. T. Imhoff, Phys. Rev. E **54**, 5575 (1996).
[10] C. Eichwald and J. Walleczek, Phys. Rev. E **55**, R6315 (1997).
[11] L. Gammaitoni, P. Häggi, P. Jung, and F. Marchesoni, Rev. Mod. Phys. **70**, 223 (1998).
[12] Gerardo J. Escalera Santos, M. Rivera, and P. Parmananda, Phys. Rev. Lett. **92**, 230601 (2004).
[13] P. Parmananda, Gerardo J. Escalera Santos, M. Rivera, and K. Showalter, Phys. Rev. E **71**, 031110 (2005).
[14] T. Amemiya, T. Ohmori, T. Yamamoto, and T. Yamaguchi, J. Phys. Chem. A **103**, 3451 (1999).
[15] E. Simonotto, M. Riani, C. Seife, M. Roberts, J. Twitty, and F. Moss, Phys. Rev. Lett. **78**, 1186 (1997).
[16] M. Ebihara, H. Mahara, T. Sakurai, A. Nomura, and H. Miike, in *Proceedings of Visualization, Imaging, and Image Processing*, Benalmadena, IASTED International Conferences No. 396, edited by H. M. Hamza (Acta, Calgary, Canada, 2003), p. 145.
[17] A. Nomura, M. Ichikawa, H. Miike, M. Ebihara, H. Mahara, and T. Sakurai, J. Phys. Soc. Jpn. **72**, 2385 (2003).
[18] D. T. Gillespie, J. Comput. Phys. **22**, 403 (1976).
[19] D. T. Gillespie, J. Phys. Chem. **81**, 2340 (1977).
[20] D. T. Gillespie, Annu. Rev. Phys. Chem. **58**, 35 (2007).
[21] Z. Hou and H. Xin, Chem. Phys. Chem **5**, 407 (2004).
[22] Z. Hou, X. T. Jun, and H. Xin, Chem. Phys. Chem **7**, 1520 (2006).
[23] Z. Wang, Z. Hou, and H. Xin, Chem. Phys. Lett. **401**, 307 (2005).
[24] S. Dey, D. Das, and P. Parmananda, CHAOS **21**, 033124 (2011).
[25] J. Elf, A. Doncic, and M. Ehrenberg, in *Proceedings of SPIE 5110, Fluctuations and Noise in Biological, Biophysical, and Biomedical Systems*, Santa Fe, 5110, SPIE (SPIE, Bellingham, WA, 2003), p. 114.
[26] T. Fricke and J. Schnakenberg, Z. Phys. B **83**, 277 (1991).
[27] J. P. Boon, D. Dab, R. Kapral, and A. Lawniczak, Phys. Rep. **273**, 55 (1996).
[28] R. Kapral and X.-G. Wu, J. Phys. Chem. **100**, 18976 (1996).
[29] A. B. Stundzia and C. J. Lumsden, J. Comp. Phys. **127**, 196 (1996).
[30] D. Bernstein, Phys. Rev. E **71**, 041103 (2005).
[31] Y. Togashi and K. Kaneko, Phyica D **205**, 87 (2005).
[32] H. Wang, Z. Fu, X. Xu, and Q. Ouyang, J. Phys. Chem. A **111**, 1265 (2007).
[33] D. T. Gillespie, L. R. Petzold, and E. Seitaridou, J. Chem. Phys. **140**, 054111 (2014).
[34] R. J. Field and R. M. Noyes, J. Chem. Phys. **60**, 1877 (1974).
[35] J. J. Tyson, Ann. N. Y. Acad. Sci. **316**, 279 (1979).

[36] A. M. Turing, Philos. Trans. R. Soc. London Ser. B **237**, 37 (1952).
[37] J. E. Pearson, Science **261**, 189 (1993).
[38] H. Mahara, K. Suzuki, R. A. Jahan, and T. Yamaguchi, Phys. Rev. E **78**, 066210 (2008).
[39] N. Kurata, H. Kitahata, H. Mahara, A. Nomura, H. Miike, and T. Sakurai, Phys. Rev. E **79**, 056203 (2009).
[40] S.-I. Ei and J. Wei, Jpn. J. Ind. Appl. Math. **19**, 181 (2002).
[41] Y. Nishiura, D. Ueyama, and T. Yanagita, SIAM J. Appl. Dyn. Syst. **4**, 733 (2005).
[42] J. V. Booth and T. Erneux, Physica A **188**, 206 (1992).
[43] A. Carpio, L. L. Bonilla, and A. Luzón, Phys. Rev. E **65**, 035207(R) (2002).
[44] J. Keener, J. Appl. Math. **47**, 556 (1986).
[45] A. Carpio and L. L. Bonilla, SIAM J. Appl. Math. **63**, 619 (2002).
[46] A. Kaminaga, V. K. Vanag, and I. R. Epstein, Angew. Chem. Int. Ed. **45**, 3087 (2006).